Journal of Power Sources 240 (2013) 328–337

Contents lists available at SciVerse ScienceDirect

Journal of Power Sources

journal homepage: www.elsevier.com/locate/jpowsour

High performance $LiFePO_4$/CN cathode material promoted by polyaniline as carbon–nitrogen precursor

Ercan Avci*, Muhsin Mazman, Davut Uzun, Emre Biçer, Tansel Şener

TUBITAK, Marmara Research Center, Energy Institute, 41470 Gebze, Kocaeli, Turkey

HIGHLIGHTS

- Pyrolysis of PANI-Cl improves the $LiFePO_4$ performance much better than sucrose.
- PANI-Cl leads to the formation of thin carbon–nitrogen layer on $LiFePO_4$ particles.
- Crosslinked polymer chains upon pyrolysis inhibit the growth of crystalline grains.
- PANI-Cl reduces the $LiFePO_4$ particle size to nanometer scale but sucrose not.

ARTICLE INFO

Article history:
Received 23 January 2013
Received in revised form
13 March 2013
Accepted 7 April 2013
Available online 18 April 2013

Keywords:
Polyaniline chloride
$LiFePO_4$
Polymer pyrolysis
Carbon–nitrogen coating
Crosslinking
Solid state synthesis

ABSTRACT

A facile and efficient solid state synthesis of carbon and nitrogen coated lithium iron phosphate ($LiFePO_4$/CN) cathode material is achieved via polymer-pyrolysis method using polyaniline-chloride (PANI-Cl). The current investigation is comparatively analyzed with the results of the composite of $LiFePO_4$/C (LFP/C) synthesized using sucrose as carbon precursor. The optimized $LiFePO_4$/CN (LFP/CN) composite is synthesized at 700 °C using 10 wt.% PANI-Cl. The composite exhibits remarkable improvement in capacity, cyclability and rate capability compared to those of LFP/C. The specific discharge capacities as high as 164 mAh g^{-1} (theoretical capacity: 170 mAh g^{-1}) at 0.1 C and 100 mAh g^{-1} at 10 C rates were achieved with LFP/CN. In addition, the composite exhibits a long-term cycling stability with the capacity loss of only 10% after 1000 cycles. PANI-Cl shifts the size distribution of the composite to nanometer scale (approximately 150 nm), however the addition of sucrose does not have such an effect. LFP/CN contains 1.6 wt.% nitrogen and 15.8 wt.% carbon. LFP particles are mostly coated with a few nanometers thick C–N layer forming a core–shell structure. The possible crosslinking mechanism of PANI-Cl upon pyrolysis on size reduction and formation of uniform carbon/nitrogen coating on LFP are also discussed.

1. Introduction

$LiFePO_4$ (LFP) is considered to be one of the most promising cathode material for the next generation high-power lithium ion batteries due to its low cost, high safety, non-toxicity and a competitive theoretical capacity [1,2]. They are envisioned to be used in electric vehicles and stationary energy storage systems for storing solar and wind power. Unfortunately, low electronic conductivity and slow diffusion of lithium ions across the two-phase boundary of LFP seriously limit its rate capability [3–6]. To overcome these intrinsic limitations, many efforts have been carried out including particle size reduction [7], doping with supervalent cations [8,9], coating with conductive polymers [6,10–12] and forming a carbon layer (LFP/C) [5,6,13–18]. Uniform carbon coating greatly enhances specific capacity, rate capacity and cycling performance of LFP [5,6]. This is due to the pyrolytic carbon in the product, which suppresses the particle growth and thus leading both particle size minimization and intimate carbon contact [19]. However, it is quite difficult to obtain a homogeneously coated carbon shell on LFP particles during the heat treatment. In case of partial formation of carbon shell, an insufficient electronically conducting network would lead to decrease in the rate capability of the material.

Previous studies mostly focused on the synthesis of LFP/C composite materials by using low weight organic precursors [20,21], such as sucrose, glucose or citric acid, as the carbon source. Although the polymer pyrolysis method is a relatively simple and effective way to form carbon-coated materials such as ceramic/carbon composites [22,23], it has been rarely applied for coating the LFP particles [12,15,19]. In such a process, pyrolized polymers can lead to the formation of reduced size LFP/C particles coated uniformly with a

* Corresponding author. Tel.: +90 262 677 2772; fax: +90 262 677 2309.
E-mail addresses: ercan.avci@tubitak.gov.tr, eavci07@yahoo.com (E. Avci).

0378-7753/$ – see front matter © 2013 Elsevier B.V. All rights reserved.
http://dx.doi.org/10.1016/j.jpowsour.2013.04.030

Table 1
Experimental conditions for the synthesis of LFP/C and LFP/CN composites and carbon and nitrogen contents determined by elemental analysis.

Notation	Material/carbon source	Sintering temperature (°C)	Carbon source (wt.%)	Contents (wt.%)		
				C	N	N/C
LFP/C	LFP/$C_{sucrose}$	700	10	8.4	–	–
LFP/CN_1	LFP/$C_{PANI-Cl}$	650	10	16.1	2.1	0.13
LFP/CN_2	LFP/$C_{PANI-Cl}$	700	10	15.8	1.6	0.10
LFP/CN_3	LFP/$C_{PANI-Cl}$	750	10	15.5	1.6	0.10
LFP/CN_4	LFP/$C_{PANI-Cl}$	700	6	12.9	1.2	0.09
LFP/CN_5	LFP/$C_{PANI-Cl}$	700	14	21.3	2.5	0.12
–	PANI-Cl	–	–	59.8	12.3	0.21

few nanometer thick carbon layers [15,19]. It is, however, important to choose the proper polymer precursor for tailoring the properties of LFP/C composite. Recently, Nien et al. [15] prepared LFP/C samples formed by calcinating amorphous LFP with various polymers such as polystyrene, polyethylene oxide, polybutadiene at 600 °C. They reported that polystyrene (5 wt.%) derivative with functionalized aromatic groups exhibited an improved performance. They achieved a capacity of 147 mAh g^{-1} and 90 mAh g^{-1} at 0.1 C and 3 C rates, respectively. Additionally, Yu and Fang [18] announced that LFP/C composite prepared using polystyrene nano-spheres (7 wt.%) sintered at 800 °C displayed a discharge capacity of 167 mAh g^{-1} and 150 mAh g^{-1} at 0.1 C and 1 C, respectively.

Polyaniline (PANI) exhibits an interesting behavior upon pyrolysis compared to many other polymers by forming a network structure as a result of crosslinking of polymer chains [24–29]. Mentus et al. reported that a disordered nitrogen-containing graphite structure is formed upon carbonization of sulfuric acid doped PANI with conductivity higher than that of pristine PANI [26]. In this article, we introduce the chloride doped PANI (PANI-Cl) as a carbon–nitrogen source for the solid state synthesis of LFP/CN composite which has very good properties as cathode material in high power lithium ion batteries. This composite seems to be a promising alternative route for an industrial-scale production due to its facile fabrication and low cost. A mixture of nanometer and micrometer size LFP/CN particles are formed as a result of the pyrolysis of PANI-Cl. It is believed that the crosslinked polymer chains inhibit the growth of crystalline grains. LFP/CN composite synthesized at 700 °C using PANI-Cl (10 wt.%) exhibits superior electrochemical performances in wide operation discharge rate range compared to LFP/C synthesized using sucrose as a carbon precursor.

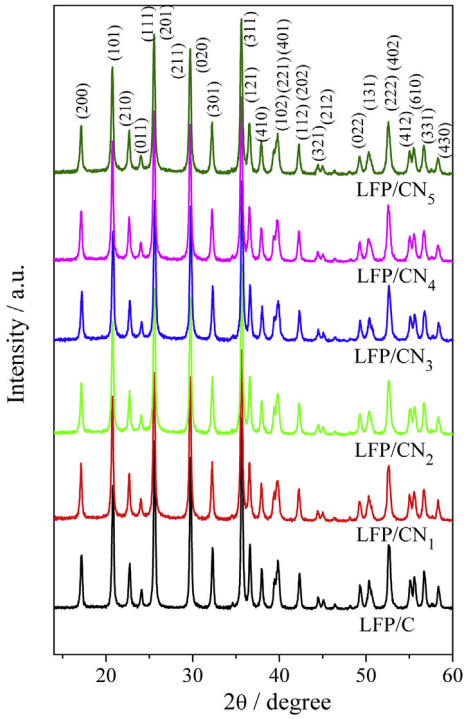

Fig. 1. XRD patterns of LFP/C and LFP/CN composites synthesized at different conditions (see Table 1).

2. Experimental

2.1. Synthesis of $LiFePO_4$/C and $LiFePO_4$/CN composites

As the starting materials for the solid-state synthesis, stoichiometric amounts of analytical grade 2.24 g of Li_2CO_3 (Alfa-Aesar), 10.99 g of $FeC_2O_4.2H_20$ (Aldrich), 6.98 g of $(NH_4)_2HPO_4$ (Carlo-Erba) as well as 2.25 g of PANI-Cl or 2.25 g of sucrose (Carlo-Erba) as carbon source precursors were thoroughly planetary milled in mortar for 2 h (300 rpm) in the mixture solvents of 30 ml of ethanol and 30 ml of N-methylpyrrolidine (NMP, Merck). The resulting gel was dried at 100 °C in a furnace and then heated to 350 °C for 6 h in

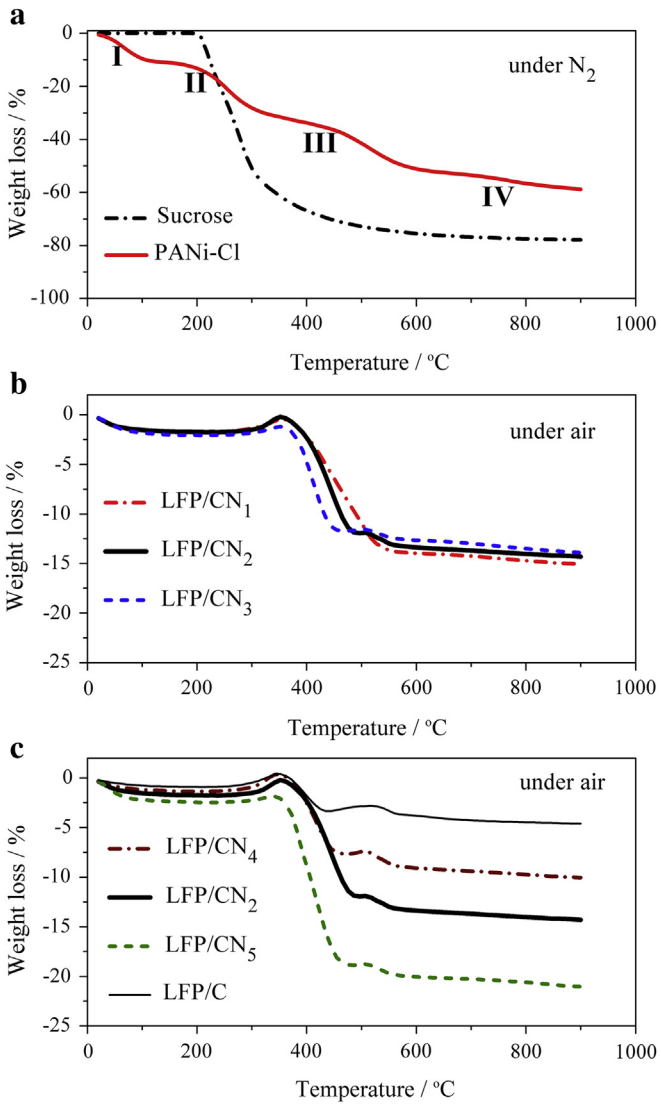

Fig. 2. Thermogravimetric curves of (a) sucrose and PANI-Cl under N_2 flow; (b) LFP/CN sintered at 650, 700, 750 °C under air, (c) LFP/CN synthesized using 6, 10, 14 wt.% PANI-Cl and LFP/C sintered at 700 °C under air.

Ar atmosphere. The decomposed mixture was pressed into pellets and sintered under Ar flow at 650, 700, or 750 °C for 12 h in order to obtain the crystalline phase composites. LFP/C precursor having 10 wt.% sucrose content was sintered at 700 °C (donated as LFP/C). Three LFP/CN samples were sintered at 650 °C, 700 °C, and 750 °C by using fixed 10 wt.% PANI-Cl donated as LFP/CN_1, LFP/CN_2, and LFP/CN_3, respectively. Other two LFP/CN samples were sintered at 700 °C by using 6 wt.% and 14 wt.% weight contents of PANI-Cl (named as LFP/CN_4, and LFP/CN_5, respectively) as shown in Table 1.

PANI-Cl used in LFP/CN materials was synthesized by oxidative polymerization of aniline-hydrochloride (Sigma-Aldrich) with ammonium peroxydisulfate (APS, Sigma) at 4:5 mol mol^{-1} ratio and excess amount of hydrochloric acid (HCl). A typical process is described as follows. First, aniline-hydrochloride (12.9 g) was dissolved in 400 ml of distilled water and stirred while keeping the mixture at 0–5 °C. A precooled APS (28.4 g) aqueous solution (400 ml) was added into the above solution together with 0.1 M HCl (200 ml) solution. The mixture was reacted for 2 h at 0–5 °C. The resulting dark green precipitate was washed several times with deionized water, ethanol and acetone, consecutively and then dried overnight at 75 °C in a vacuum oven. Under the present condition, the synthesis of high degree crystalline of PANI-Cl having molecular weight around 85 000 is expected [30].

2.2. Characterization of cathode materials

The crystallographic structural characterization was performed by X-ray powder diffraction. XRD of the LFP/C and LFP/CN composites were carried out on a Rigaku Miniflex 600 diffractometer equipped with Cu-Kα radiation of $\lambda = 0.15405$ nm in the range of $0° < 2\theta < 80°$. The micromorphology of the LFP/C powders was observed using a JEOL JSM6510-LV scanning electron microscope (SEM). Transmission electron microscopy (TEM) measurements were performed using JEOL JEM 2100 HRTEM operating at 200 kV (LaB6 filament) with Oxford Instruments X-Sight 6498 energy dispersive spectroscopy (EDS) and selected-area electron diffraction (SAED) systems. The carbon content was estimated from a Leco (TruSpec) elemental analyzer and thermogravimetric analysis (Mettler-Toledo TGA-851). Particle size analysis (PSA) of the composites was investigated by dispersing the materials in water using Malvern Mastersizer-2000.

2.3. Cell fabrication and electrochemical measurements

The crystalline cathode active materials of LFP/CN or LFP/C were mixed and grounded with Super P (12 wt.%, Timcal Co.) and polyvinylidene fluoride (PVdF, 8 wt.%) as a binder dissolving in NMP for 30 min. The resulting mixture was casted uniformly onto an aluminum foil and dried at 100 °C. Electrodes were punched in the form of a disc having 3–4 mg cm^{-2} of active material, pressed and dried at 100 °C for 4 h. The coin cells (CR2032) were assembled in an argon-filled glove-box (Vigor) with a Li metal disc as anode and Whatman GF/D glass-fiber as separator and 1 M $LiPF_6$ in a mixture of ethylene carbonate (EC) and diethyl carbonate (DEC) (1:1 in vol. ratio) as the electrolyte. Cyclic voltammograms (CV) (between 2.0 and 4.3 V) and galvanostatic charge/discharge measurements were carried out (between 2.2 and 4.2 V) with PAR VersaSTAT Multi channel potentiostat/galvanostat. After each charging step, the cells were further recharged holding at 4.0 V for 10 min to recover their full capacity before applying a subsequent discharge step.

3. Results and discussion

3.1. Material characterization

XRD patterns of the LFP/C powders prepared using different concentrations of sucrose and PANI-Cl at varying sintering temperatures are shown in Fig. 1. All peaks on each curve can be

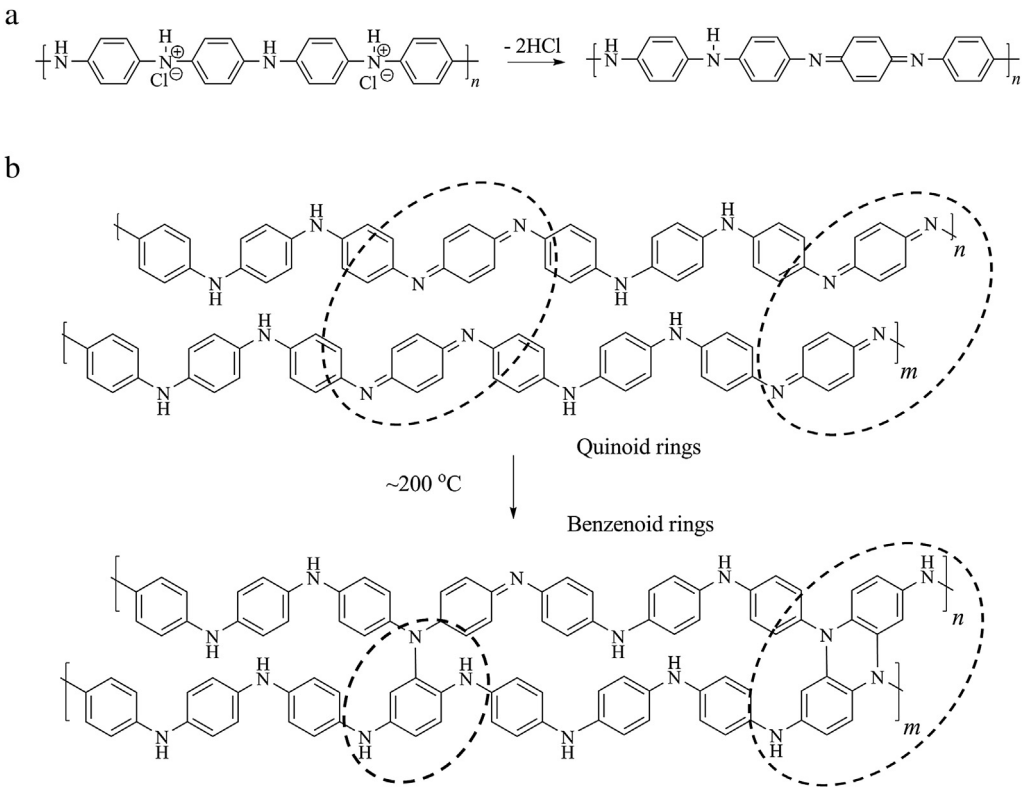

Fig. 3. (a) Dehydrochlorination of PANI-Cl, (b) crosslinking chemical reaction of dehydrochlorinated PANI-Cl chains during heat treatment [24,26,27].

indexed as a single phase with an ordered orthorhombic olivine structure with a space group Pmnb (ICDD (PDF-2/Release 2011 RDB) DB card number: 01-074-9597) indicating the successful synthesis of phase-pure $LiFePO_4$ (lattice parameters: $a = 10.321$ Å, $b = 6.008$ Å, $c = 4.692$ Å). Crystallite sizes calculated according to Williamson-Hall method vary between 25 and 28 nm.

Sucrose and PANI-Cl were thermally analyzed in order to examine the effect of their pyrolysis on the formation of LFP/C and LFP/CN composites as shown in Fig. 2(a). The samples were heated from 25 °C to 900 °C at a rate of 10 °C min^{-1} under N_2 flow (40 ml min^{-1}). The pyrolysis of sucrose takes place at single step starting at 200 °C and sucrose losses 75% of its weight till 700 °C. On the other hand, the pyrolysis of PANI-Cl proceeds at four steps. The first step at temperatures up to 150 °C is possibly due to the loss of unbound water (~10 wt.%). The second step in the temperature range of 150–350 °C is attributed to the loss of HCl (dehydrochlorination, ~20 wt.%), ammonia and bound water [26,28,29]. The reaction scheme of dehydrochlorination of PANI-Cl taking place at this heating step is shown in Fig. 3(a). Around 200 °C, dehydrochlorinated PANI-Cl chains undergo both intermacromolecular and intramacromolecular crosslinking processes [24–29]. As a result of crosslinking, nearly complete conversion of quinoid rings to benzenoid rings takes place as shown in Fig. 3(b) [24,27] The weight loss at the third step (~21 wt.%) between 350 and 600 °C might be the result of the degradation of the crosslinked structures, polymer chain break into extended aromatic fragments (benzene, aniline, diphenylamine, other greater oligomers [31]) as well as ammonia removal. The forth step at the temperatures over 600 °C (~5 wt.%) may be due to the degradation of the crosslinked structures and polymer backbone [26,32].

To determine the amount of carbon in the composites, TGA was carried out in air (40 ml min^{-1}) at a heating rate of 10 °C min^{-1} (Fig. 2(b,c)) in addition to the elemental analysis. The percent carbon amounts determined by elemental analysis (Table 1) are close to those of obtained from TGA experiments. At this point, it is worth noting that the oxidation of Fe(II) to Fe(III) (formation of iron oxides) which is observed at temperature ranges between 350 and 500 °C leads to an increase of 4.8 wt.% for the retained mass of composites [33,34]. Considering both elemental analysis and TGA, carbon contents of LFP/C and LFP/CN_2 were measured as 8.4 and 15.8 wt.%, respectively. It is also important to note that the weight loss of sucrose and PANI-Cl during the active material preparation (~62 wt.% for LFP/C, ~25 wt.% for LFP/CN_2) is lower than that during the pyrolysis of these carbon sources during TGA experiment (~75 wt.% for sucrose, ~55 wt.% for PANI-Cl). This indicates that some of volatile pyrolysis products of sucrose and PANI-Cl stick to the composite wall without leaving the material and this might help the formation of more uniform carbon or carbon–nitrogen shell around particles. Another important point to notice is the low ratio of residual weight of nitrogen over residual weight of carbon (N/C) in LFP/CN composites compared to that of pristine PANI-Cl (Table 1). This shows that the removal of ammonia and other nitrogen containing pyrolysis products takes place more readily compared to the carbon containing products.

Fig. 4 shows the particle size distributions of pyrolized forms of carbon sources, LFP/C and LFP/CN samples. The distribution of pyrolized PANI-Cl is narrow and centered on ~10 μm, whereas the distribution for the pyrolized sucrose is broad and centered on ~100 μm (Fig. 4(a)). The distribution shifts to smaller sizes (centered on ~3 μm) for LFP/C composite compared to that of pyrolized sucrose. Size distributions of LFP/CN composites prepared at different conditions exhibit an interesting behavior localizing at two regions (Fig. 4(b,c)). One distribution region is

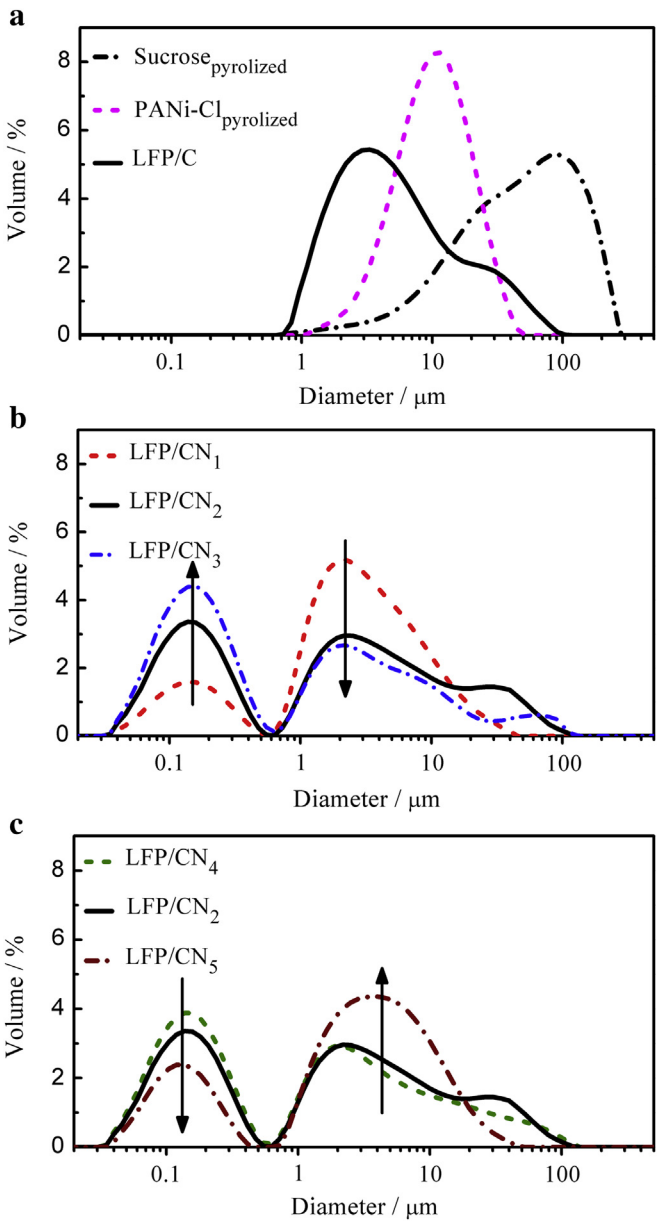

Fig. 4. Particle size distributions of (a) sucrose and PANI-Cl pyrolized at 350 °C (6 h), 700 °C (12 h) under Ar flow and LFP/C; (b) LFP/CN sintered at 650, 700, 750 °C, (c) LFP/CN synthesized using 6, 10, 14 wt.% PANI-Cl.

centered on ~150 nm. On the other hand, another region is centered on ~2 μm. The borders of those regions do not change with the synthesis conditions, such as sintering temperature or the weight content of PANI-Cl in the precursor. However, the number of particles in these regions strictly depends on the synthesis conditions. The number ratio of submicrometer LFP/CN particles increases with sintering temperature (Fig. 4(b)) and decreases surprisingly with the content of PANI-Cl in the precursor (Fig. 4(c)). The distributions clearly reveal that PANI-Cl restricts the growth of the composite particles, but this result does not mean that higher content of PANI-Cl would lead to the formation of smaller particles. Approximately, 40 vol.% of LFP/CN_2 particles are below 500 nm in diameter, whereas most of LFP/C particles are larger than 1 μm in diameter.

The morphology of the composites was characterized by SEM. Fig. 5 shows the SEM images of LFP/CN and LFP/C composites

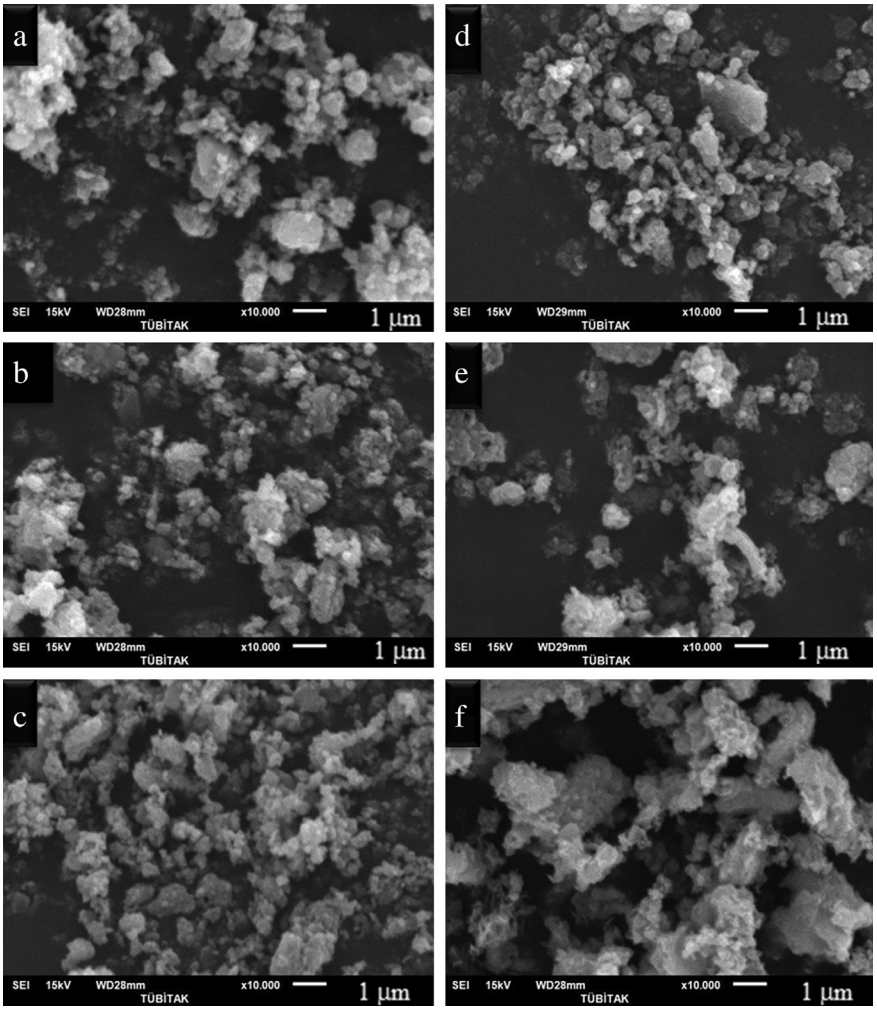

Fig. 5. SEM images of (a–c) LFP/CN composites sintered at 650, 700, 750 °C (10 wt.% PANI-Cl); (d,e) LFP/CN synthesized using 6, 14 wt.% PANI-Cl sintered at 700 °C, respectively; and (f) LFP/C sintered at 700 °C.

synthesized at different conditions. The micrographs exhibit mostly a similar characteristic as those of the particle size analysis (PSA, Fig. 4). LFP/CN composites appear to have both nanometer and micrometer grain size with irregular morphology (Fig. 5(a–e)). However, LFP/C particles are mostly in micrometer size (Fig. 5(f)). As the sintering temperature of LFP/CN increases from 650 to 750 °C, formation of nanometer size particles becomes dominant as shown Fig. 5(a–c). This indicates that the particles become more pulverized with temperature. Similar to PSA results, higher content of PANI-Cl results in larger composite particle as observed in the micrographs (Fig. 5(b,d,e)). Both PSA and SEM results reveal that carbon–nitrogen coating via pyrolysis of PANICl plays an important role in controlling the growth of particles. The reduced particle size results in shortening of the diffusion path of Li^+ and hence better electrochemical performance of LFP/CN compared to that of LFP/C. This is further supported by the electrochemical measurements described below.

To confirm how the carbon is dispersed within LFP powder, the nanoscale microstructures of LFP/C and LFP/CN_2 composites are further studied using TEM, SAED and EDS methods as shown in Fig. 6 and Fig. 7, respectively. There are discrete carbon layers coating on both LFP particles as shown in Fig. 6(a–d) and Fig. 7(a–d). One of the common features of the TEM images of both samples is that large carbon segments are located between large LFP particles (Fig. 6(a) and Fig. 7(a)). The EDS/SAED spectra in Fig. 6(e–h) and Fig. 7(e–h) indicate the presence of crystalline $LiFePO_4$ (darker regions) and abundant amorphous carbon phases. However, a few weak spots in addition to hollow ring observed in the SAED pattern of LFP/CN (Fig. 7(f)) indicate the presence of some crystalline carbon phase. This crystalline carbon phase is possibly due to the aromatic pyrolysis products. The images at higher magnification (Fig. 6(d) and Fig. 7(d)) demonstrate that the coating is extended over the surfaces of LFP particles forming a core–shell structure. Thicknesses of the shells are measured as 3.1 nm and 1.6 nm for the samples of LFP/C and LFP/CN_2, respectively. The complete carbon coating around or between the particles is expected to contribute to the improved electrochemical properties of the composites.

Considering the results derived from PSA, SEM and TEM methods, the possible explanation for the size reduction effect of PANI-Cl can be given in Fig. 8. In this scheme, PANI-Cl was first mixed with LFP precursors, followed by heating at 350 °C for 6 h. During this heating period, calcination of the precursors and the crosslinking of PANI chains occur. Upon pyrolysis, formation of low degree and high degree crosslinked of PANI network structure is expected. The product was further subjected to heat treatments in the range 650 °C–750 °C under N_2 atmosphere to sinter the LFP and carbonize PANI. At this heating stage, PANI chains break into

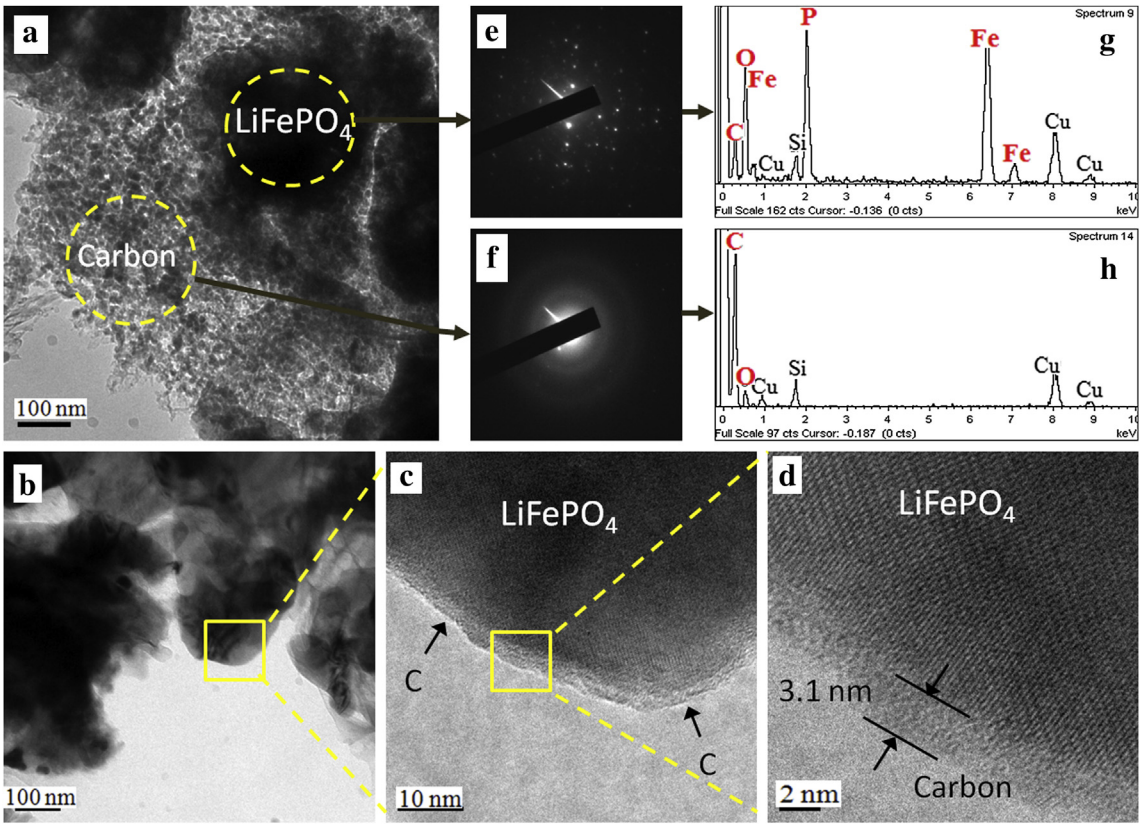

Fig. 6. (a–d) TEM and HRTEM images of LFP/C composite particles; (e,f) SAED patterns for the particles; (g,h) EDS analyses for the particles.

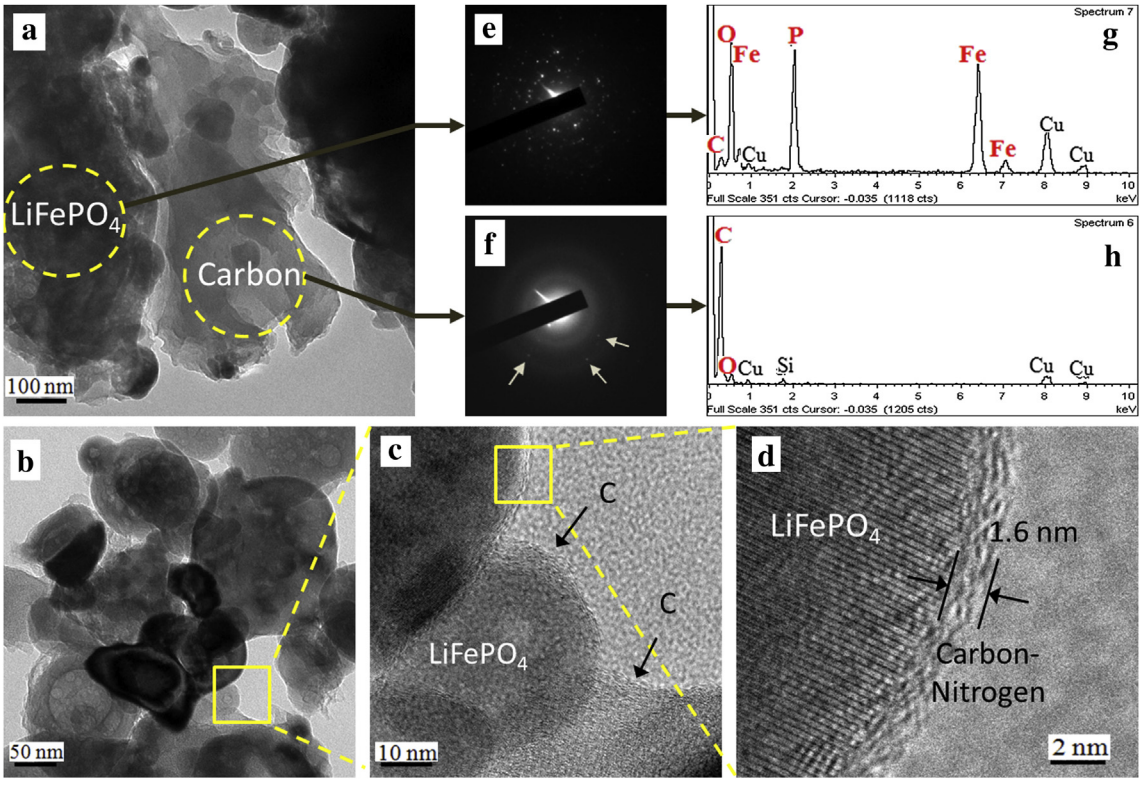

Fig. 7. (a–d) TEM and HRTEM images of LFP/CN_2 composite particles; (e,f) SAED patterns for the particles; (g,h) EDS analyses for the particles.

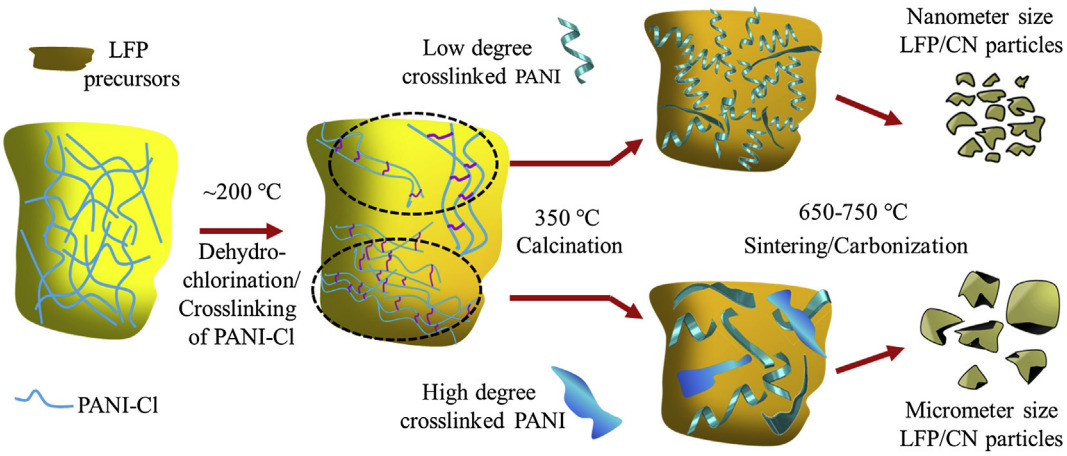

Fig. 8. Schematic diagram of formation of nanometer and micrometer size LFP/CN composite.

aromatic fragments, while lower weight volatile fragments leave the composite, heavier volatile fragments are not able to leave the material and possibly stick to the wall of the composite. Additionally, as the high degree crosslinked PANI products form relatively larger size C–N segments around micrometer size LFP particles, low degree crosslinked products mostly surround relatively smaller size LFP particles forming nanometer size LFP/CN particles.

3.2. Electrochemical measurements

Fig. 9 shows the cyclic voltammogram (CV) curves of LFP/CN sintered at different temperatures and different concentrations of PANI-Cl precursors scanned at a rate of 0.1 mV s^{-1}. All samples, except the sample of LFP/CN_5 synthesized using the highest PANI-Cl weight content, reveal the single-electron reaction mechanism indicating the characteristic redox behavior of $LiFePO_4$ cathode material. However, in comparison with the samples having less PANI-Cl content (LFP/CN_2 and LFP/CN_4), LFP/CN_5 composite (21.8 wt.% carbon) possess two broad oxidation peaks located at 3.6 and 4.0 V and a single broad reduction peak at 3.2 V.

Fig. 10 shows the results of cyclability tests of LFP/C and LFP/CN electrodes at the discharging rate ranging from 0.2 C to 10 C (1 C = 170 mAh g^{-1}). In Fig. 10(a), the effect of various sintering temperatures (650, 700 and 750 °C) on cyclability of LFP/CN electrodes is demonstrated (using 10 wt.% PANI-Cl). Clearly, the highest discharge capacities at all C-rates are obtained from the electrode of LFP/CN_2 sintered at 700 °C (0.2 C: 163 mAh g^{-1}, 1 C: 148 mAh g^{-1}, 10 C: 100 mAh g^{-1}), whereas the lowest capacities are observed at the electrode material sintered at 750 °C (LFP/CN_3). Although LFP/CN_3 contains almost the same amount of carbon and nitrogen (see Table 1) as well as its particles are smaller (Fig. 4(b), Fig. 5(b,c)) compared to LFP/CN_2 material, it exhibits a lower electrochemical performance. The reason behind this contradiction can be attributed to the blocking in 1D channels where the Li^+ ions move in $LiFePO_4$ crystal as a result of the formation of undesired impurities such as Fe_2P, Fe_2O_3, $Li_3Fe_2(PO_4)_3$ or antisite defects [35]. When the XRD patterns (Fig. 1) are examined closely, impurity phases are not encountered. Therefore, the formation of antisite defects as a result of the higher reaction temperature seems to be the stronger reason behind the formation of blocked channels as well as lower electrochemical performance. To find out the effect of concentration of PANI-Cl on the cyclability of LFP/CN electrodes, the sintering temperature is fixed at 700 °C and three different precursors having 6, 10 and 14 wt.% PANI-Cl (LFP/CN_4, LFP/CN_2 and LFP/CN_5, respectively) were investigated (Fig. 10(b)). Substantially, the performance was not necessarily better with higher carbon contents. It is clear that 10 wt.% PANI-Cl content in the precursor is the optimal value among the prepared samples and results in the highest discharge capacities at the rate ranging from 0.2 C to 10 C. The sample having the highest carbon content (LFP/CN_5) has the lowest capacity at low rates, but surprisingly has relatively higher capacity at high 10 C rate. The rapid decrease of performance at low rates

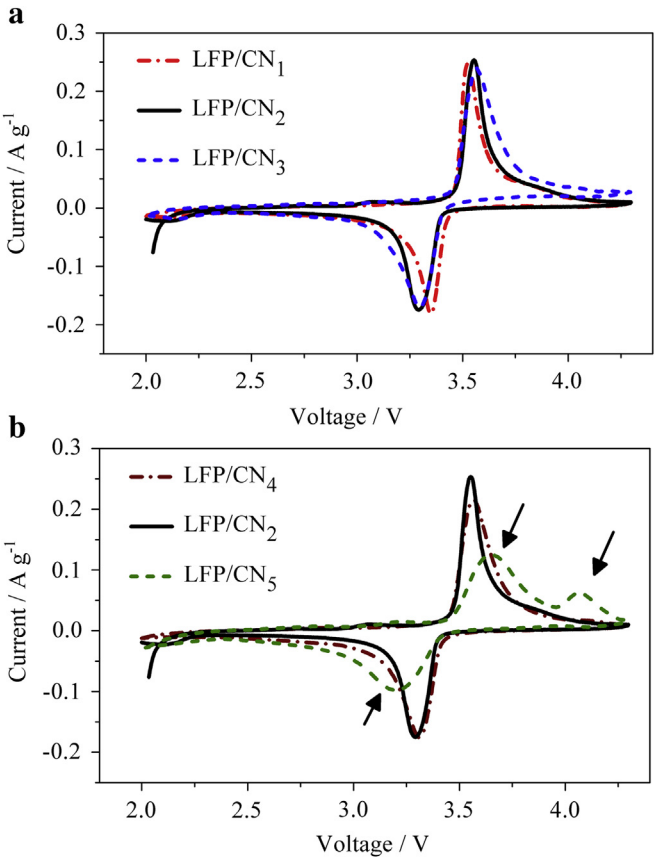

Fig. 9. CV curves of LFP/CN composites (a) sintered at 650, 700, and 750 °C, (b) using 6, 10, and 14 wt.% PANI-Cl sintered at 700 °C at scan rate of 0.1 mV s^{-1}.

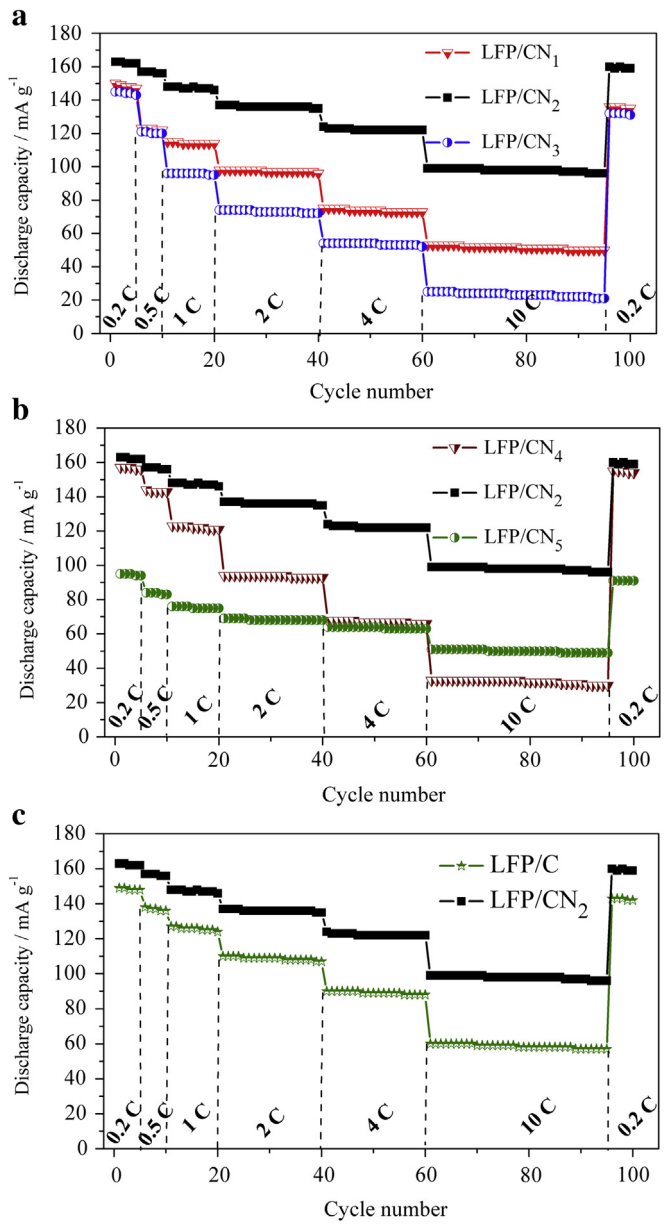

Fig. 10. Rate capability of (a) LFP/CN composites (10 wt.% PANI-Cl) sintered at 650, 700, and 750 °C, (b) LFP/CN composites synthesized using 4, 10, and 14 wt.% PANI-Cl sintered at 700 °C, and (c) LFP/C and LFP/CN_2 (10 wt.%) sintered at 700 °C.

can be attributed to the formation of excessive amorphous carbon phase diluting the density of the crystalline LFP phase and the suppression of the formation of crystalline LFP phase by excess carbon [36].

In Fig. 10(c), the cyclability performances of LFP/C and LFP/CN_2 electrodes are compared based on varying discharging rates. In comparison to LFP/C composite, LFP/CN_2 composite demonstrates a promising capacity, cyclability, and rate performance. The specific discharge capacities as high as 163 mAh g^{-1} at 0.2 C, 100 mAh g^{-1} at 10 C rates with a 2% capacity fading after 100 cycles were obtained for LFP/CN_2. On the other hand, LFP/C exhibits the specific discharge capacities of 149 mAh g^{-1} at 0.2 C, 60 mAh g^{-1} at 10 C rates with the capacity fading of 5% after 100 cycles. This excellent electrochemical performance of LFP/CN_2 implies that the coating of LFP surface with pyrolyzed PANI-Cl facilitates the electrochemical insertion/extraction process of Li^+ ion, especially at high rate.

Cyclic voltammetry was used to examine the kinetics of lithium intercalation and de-intercalation. Fig. 11(a) and (b) shows the CV curves of LFP/C and LFP/CN_2 at an increasing scan rate from 0.1 to 2 mV s^{-1}, respectively. It is clear that the intensity and the area under the redox peaks for both composites increases with the scan rate. Using Randles Sevcik equation, $i_p = 2.69 \times 10^5 n^{3/2} A D^{1/2} C \nu^{1/2}$, the linear dependence of peak current (i_p) of CV of samples on the square root of scan rate ($\nu^{1/2}$) can be observed in Fig. 11(c). Considering the parameters of A (electrode area), C (concentration of Li^+) and n (number of electrons involved in the redox process) are fixed values for both electrodes, the diffusion coefficient of lithium (D_{Li}) of LFP/CN_2 is found to be 1.35 times higher than that of LFP/C. This indicates that the coating of LFP with carbon and nitrogen originating from PANI-Cl is more uniform and it improves transportation of Li ions during cell operation.

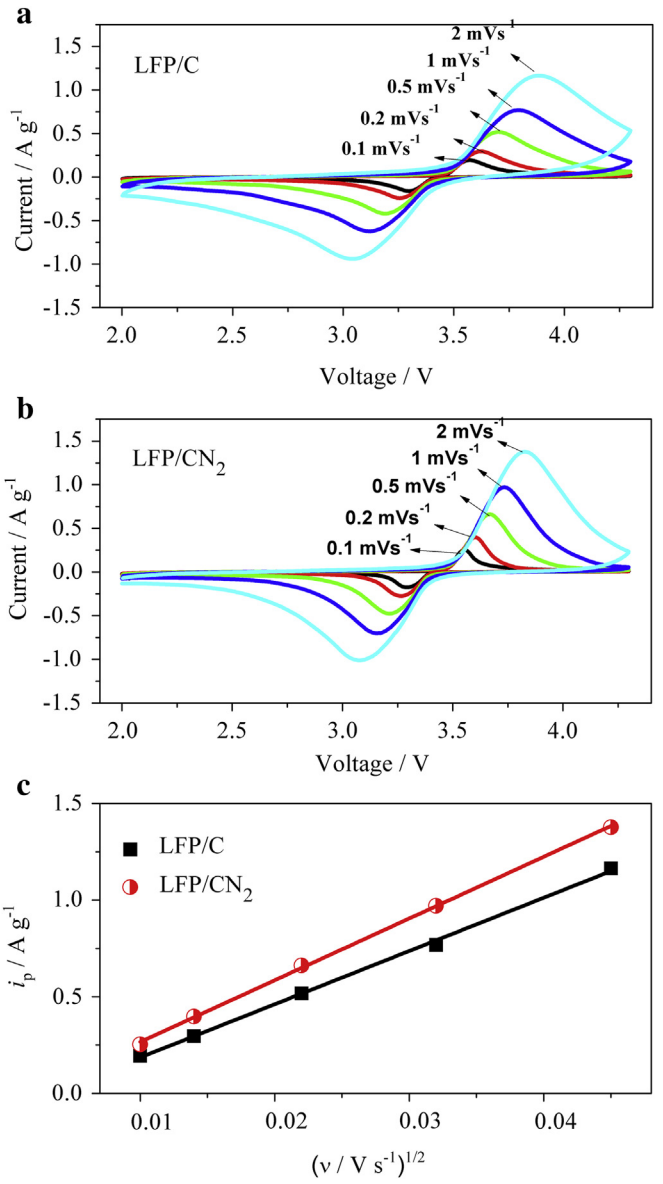

Fig. 11. CV curves of (a) LFP/C and (b) LFP/CN sintered at 700 °C, at various scan rates. (c) The relationship of peak current (i_p) and the square root of scan rate ($\nu^{1/2}$) for both samples.

Fig. 12(a,b) presents the galvanostatic charge–discharge voltage profiles of cells containing LFP/C and LFP/CN_2 at the increasing rate from 0.2 C to 10 C between 2.2 and 4.2 V vs. Li^+/Li. Both samples exhibit typical flat charge-discharge plateaus at approximately 3.4 V implying the Fe^{2+}/Fe^{3+} redox reaction. As shown in Fig. 12(a), the initial discharge capacity of LFP/C is around 150 mAh g^{-1} at 0.2 C rate, whereas LFP/CN_2 exhibits a higher discharge capacity of 163 mAh g^{-1} at the same condition. At higher C-rates, again LFP/CN_2 composite demonstrates a superior performance compared to the LFP/C sample. As shown in Fig. 12(c), it is clear that LFP/CN_2 demonstrates a slower enlargement in voltage polarization compared to the LFP/C sample as the C-rate increases.

Long term cycling capability of LFP/CN_2 sample is tested at varying C-rates as shown in Fig. 13. The initial discharge capacity of the composite is 164 mAh g^{-1} at 0.1 C and found to decay gradually with continuous cycling at increasing rates, retaining 148 mAh g^{-1} at 0.1 C after 1000 cycles suffering only 10% capacity loss. Such a superior electrochemical performance surely can satisfy the power requirements of electric vehicles [37].

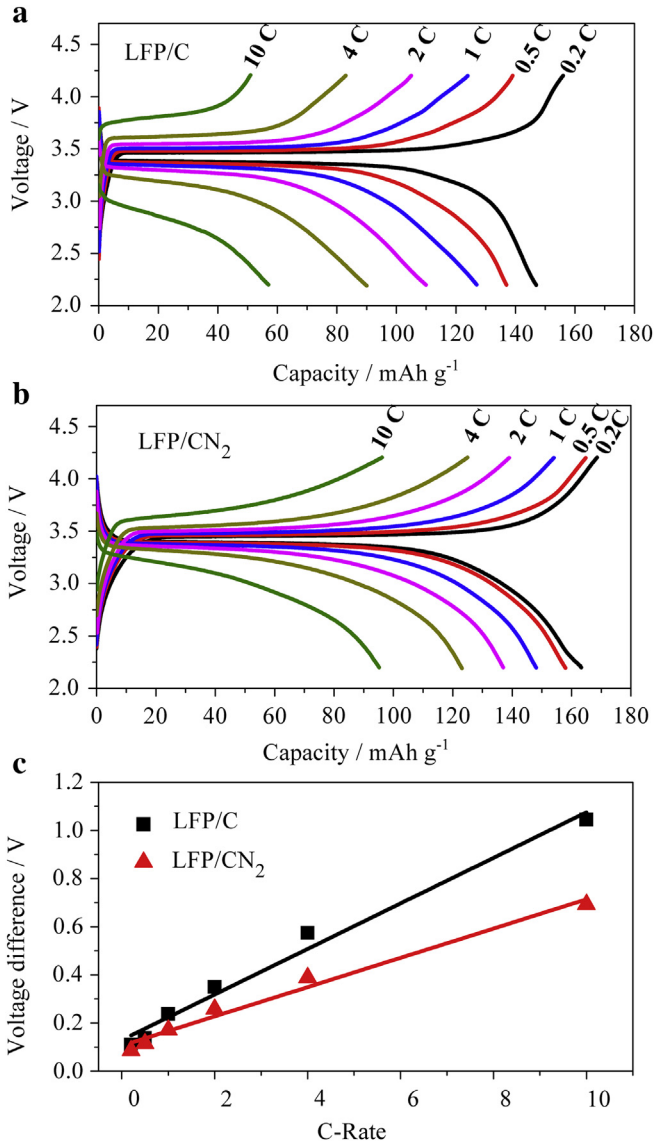

Fig. 12. Charge–discharge profiles of (a) LFP/C and (b) LFP/CN_2 (10 wt.% PANI-Cl) sintered at 700 °C. (c) The dependence of voltage difference between charging and discharging at half capacity on C-rate for both samples.

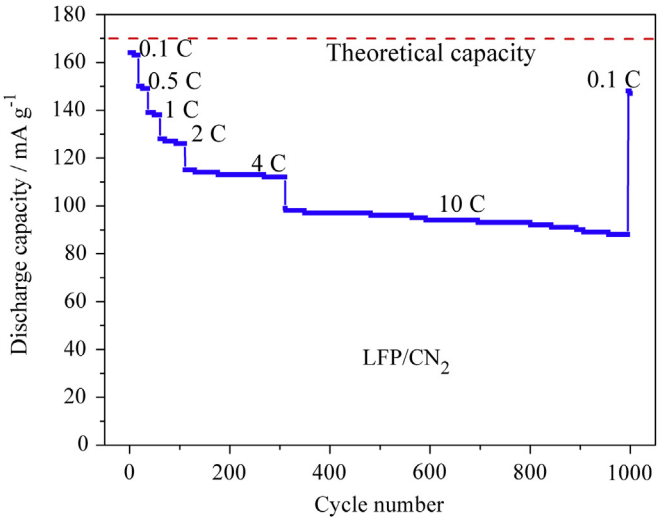

Fig. 13. Cyclability performance (1000 cycle) of LFP/CN_2 synthesized using 10 wt.% PANI-Cl sintered at 700 °C.

4. Conclusions

With a simple and efficient way, the mixture of nanometer and micrometer size LFP/CN composite was successfully prepared using PANI-Cl as carbon nitrogen precursor. Crosslinking of PANI-Cl upon pyrolysis possibly leads to size reduction and formation of complete carbon–nitrogen coating on LFP. The amount of PANI-Cl in the precursor and the sintering temperature has significant effects on the physical and electrochemical properties of the composites. The optimized LFP/CN is prepared using 10 wt.% PANI-Cl and sintered at 700 °C, which contains 1.6 wt.% nitrogen in addition to 15.8 wt.% carbon. The LFP/CN composite exhibits a higher electrochemical performance compared with LFP/C composite synthesized using sucrose. LFP/CN particles are mostly covered with a few nanometer thick carbon–nitrogen layer, forming a core–shell structure. The specific discharge capacities of 164 mAh g^{-1} at 0.1 C, 100 mAh g^{-1} at 10 C rates with a 2% capacity fading after 100 cycles were achieved. Besides, the composite exhibits a long-term cycling stability with the capacity loss of only 10% beyond 1000 cycles.

Acknowledgments

The authors thank to The Scientific and Technological Research Council of Turkey (TUBITAK) for the financial support under the COST programme (contract no. 111T567). Thanks are also to M.Sc. Serkan Gürbüz for XRD measurements and M.Sc. Berrin Engin for TGA experiments.

References

[1] A.K. Padhi, K.S. Nanjundaswamy, J.B. Goodenough, J. Electrochem. Soc. 144 (1997) 1188–1194.
[2] N. Terada, T. Yanagi, S. Arai, M. Yoshikawa, K. Ohta, N. Nakajima, N. Arai, J. Power Sources 1–2 (2001) 80–92.
[3] A.S. Andersson, B. Kalska, L. Haggstrom, J.O. Thomas, Solid State Ionics 130 (2000) 41–52.
[4] N. Ravet, Y. Chouinard, J.F. Magnan, S. Besner, M. Gauthier, M. Armand, J. Power Sources 97–98 (2001) 503–507.
[5] B.L. Ellis, K.T. Lee, L.F. Nazar, Chem. Mater. 22 (2010) 691–714.
[6] J. Wang, X. Sun, Energy Environ. Sci. 5 (2012) 5163–5185.
[7] P. Gibot, M.C. Cabanas, L. Laffont, S. Levasseur, P. Carlach, S. Hamelet, J.M. Tarascon, C. Masquelier, Nat. Mater. 7 (2008) 741–747.
[8] H. Goktepe, H. Sahan, A. Ulgen, S. Patat, J. Mater, Sci. Technol. 27 (2011) 861–864.
[9] Y. Lin, Y. Lin, T. Zhou, G. Zhao, Y. Huang, Z. Huang, J. Power Sources 226 (2013) 20–26.

[10] W.M. Chen, Y.H. Huang, L.X. Yuan, J. Electroanal. Chem. 660 (2011) 108–113.
[11] W.M. Chen, L. Qie, L.X. Yuan, S.A. Xia, X.L. Hu, W.X. Zhang, Y.H. Huang, Electrochim. Acta 56 (2011) 2689–2695.
[12] J. Liu, G. Yang, X. Zhang, J. Wang, R. Wang, J. Power Sources 197 (2012) 253–259.
[13] S.Y. Chung, J.T. Blocking, Y.M. Chiang, Nat. Mater. 1 (2002) 123–128.
[14] Y. Wang, Y. Wang, E. Hosono, K. Wang, H. Zhou, Angew. Chem. Int. Ed. 47 (2008) 7461–7465.
[15] Y.H. Nien, J.R. Carey, J.S. Chen, J. Power Sources 193 (2009) 822–827.
[16] G.T. Kuo Fey, T.L. Lu, J. Power Sources 178 (2008) 807–814.
[17] K. Yang, Z. Lin, X. Hu, Z. Deng, J. Suo, Electrochim. Acta 56 (2011) 2941–2946.
[18] S. Yu, S. Dan, G. Luo, W. Liu, Y. Luo, X. Yu, Y. Fang, J. Solid State Electrochem 16 (2012) 1675–1681.
[19] Y. Wang, Z. Liu, S. Zhou, Electrochim. Acta 58 (2011) 359–363.
[20] D. Zhang, X. Yu, Y. Wang, R. Cai, Z. Shao, X.Z. Liao, Z.F. Ma, J. Electrochem. Soc. 156 (2009) A802–A808.
[21] H. Goktepe, H. Sahan, F. Kılıc, S. Patat, Ionics 16 (2010) 203–208.
[22] B. Ozkal, W. Jiang, O. Yamamoto, K. Fuda, Z.E. Nakagawa, J. Mater. Sci. 42 (2007) 983–988.
[23] J. Hacaloglu, T. Ersen, N. Ertugrul, M.M. Fares, S. Suzer, Eur. Polym. J. 33 (1997) 199–203.
[24] R. Mathew, B.R. Mattes, M.P. Espe, Synth. Met. 131 (2002) 141–147.
[25] X. Zhi, G. Liang, L. Wang, X. Ou, J. Zhang, J. Cui, J. Power Sources 189 (2009) 779–782.
[26] S. Mentus, G.C. Marjanovic, M. Trchova, J. Stejskal, Nanotechnology 20 (2009) 245601–245610.
[27] S. Bhadra, D. Khastgir, Polym. Degrad. Stab. 93 (2008) 1094–1099.
[28] W.F. Alves, E.C. Venancio, F.L. Leite, D.H.F. Kanda, L.F. Malmonge, J.A. Malmonge, L.H.C. Mattoso, Thermochim. Acta 502 (2010) 43–46.
[29] T. Chen, C. Dong, X. Li, J. Gao, Polym. Degrad. Stab. 94 (2009) 1788–1794.
[30] H.S. Kolla, S.P. Surwade, X. Zhang, A.G. MacDiarmid, S.K. Manohar, J. Am. Chem. Soc. 127 (2005) 16770–16771.
[31] S. Borros, E. Munoz, I. Folch, J. Chromatogr. A 837 (1999) 273–279.
[32] G.M.D. Nascimento, C.H.B. Silva, M.L.A. Temperini, Polym. Degrad. Stab. 93 (2008) 291–297.
[33] S.F. Yang, Y.N. Song, P.Y. Zavalij, M.S. Whittingham, Electrochem. Commun. 4 (2002) 239–244.
[34] M.M. Rahman, J.Z. Wang, R. Zeng, D. Wexler, H.K. Liu, J. Power Sources 206 (2012) 259–266.
[35] L.X. Yuan, Z.H. Wang, W.X. Zhang, X.L. Hu, J.T. Chen, Y.H. Huang, J.B. Goodenough, Energy Environ. Sci. 4 (2011) 269–284.
[36] S.S. Zhang, J.L. Allen, K. Xua, T.R. Jow, J. Power Sources 147 (2005) 234–240.
[37] E. Baker, H. Chon, J. Keisler, Technol. Forecast. Soc. 77 (2010) 1139–1146.